Quantum Dynamics at the State-to-State Level of the C + OH Reaction on the First Excited Potential Energy Surface†

M. Jorfi and P. Honvault*

Institut UTINAM UMR CNRS 6213, University of Franche-Comté, 25030 Besançon Cedex, France

Received: September 16, 2009; Revised Manuscript Received: October 15, 2009

Total and state-to-state reaction probabilities for the $C(^3P) + OH(X^2\Pi) \rightarrow CO(a^3\Pi) + H(^2S)$ reaction on the first excited potential energy surface of $1^2A''$ symmetry have been calculated using an accurate time-independent quantum-mechanical method at a total angular momentum $J = 0$. The total reaction probability presents a dense resonance structure that was not observed on the ground potential energy surface. The vibrational distributions appear flat or inverted, depending on the collision energy. The rotational distributions show no specific behavior. The rate constant calculated in the J-shifting approach is in good agreement with a previous theoretical result obtained using a quasi-classical trajectory method.

Introduction

Recently, we have performed quantum-mechanical (QM) and quasi-classical trajectory (QCT) calculations for the O + OH[1−4] and N + OH[5−7] reactions. We have also investigated the structure and dynamics of the $C(^3P) + OH(X^2\Pi) \rightarrow CO(X^1\Sigma^+) + H(^2S)$ reaction on the ground X^2A' potential energy surface (PES) built by our group[8] using a QCT method[9−11] or a time-dependent wave packet (TDWP) method.[12,13] The HCO complex has been the object of previous studies concerning its photodissociation process through the X^2A'-A^2A'' Renner−Teller coupling.[14,15] The collision studies suggest that the reaction is mainly dominated by a direct mechanism in which a very short lived intermediate complex is involved, despite the large well depth (7.3 eV relative to the entrance channel) in the potential. Recently, our group performed ab initio calculations[11] at the multireference internally contracted single and double configuration interaction level plus Davidson correction. Analytical global PESs have been generated using the "Reproducing Kernel Hilbert Space" method for the $1^2A''$ and $1^4A''$ states, which correlate to the $C(^3P)$ + OH entrance channel and to the $CO(a^3\Pi) + H(^2S)$ excited product channel. The ab initio calculations[11] have shown that the entrance channel of the $2^2A'$ state has a barrier larger than 0.2 eV for all angular approaches and the $1^4A'$ state forms a nonreactive complex. The rate constants of the C + OH reaction and their temperature dependence have been determined[11] on each of the three adiabatic electronic states—X^2A', $1^2A''$, and $1^4A''$—using a QCT method. Because of the huge number of quantum states due to the two heavy atoms (C and O) and the deep potential well, an accurate quantum mechanical characterization of the reaction dynamics is a challenge, particularly for state-to-state attributes. In the present work, we consider the QM dynamics at the state-to-state level on the $1^2A''$ first excited electronic state for a total angular momentum $J = 0$.

The entrance channel of the $1^2A''$ state is very similar to the ground state's with no entrance barrier. The first excited state is characterized by two minima and two saddle points located energetically above those of the ground state. The global minimum is found for HCO at linearity with an energy of −6.16 eV relative to the entrance channel. This minimum is degenerate with the HCO inversion saddle point of the ground PES, leading to a Renner−Teller coupling between the two states, which is not taken into account in this work. The other minimum is found for the COH conformation with an energy of −4.63 eV relative to the entrance channel. The first saddle point, associated with the isomerization barrier between the two conformations, lower than the exit channel, has an energy of −3.11 eV relative to the entrance channel and −2.80 eV relative to the exit channel. The last saddle point corresponds to the inversion barrier of COH and has an energy of −4.34 eV relative to the entrance channel. A competition between direct (COH) and indirect (HCO) mechanisms may be therefore possible on the $1^2A''$ state. Although the $1^2A''$ PES has similarities with the ground PES, there is a large difference between the two states concerning the exoergicity ΔH_0^0 of the C + OH reaction, which is 6.5 eV (between the entrance and exit channels) for the X^2A' state, but only 0.41 eV for the excited state. Other features and details of the $1^2A''$ PES are given in ref 11.

QM total reaction probability, vibrationally and rotationally product state-resolved reaction probabilities, vibrational and rotational product distributions at $J = 0$, and the rate constant for the $C(^3P) + OH(X^2\Pi) \rightarrow CO(a^3\Pi) + H(^2S)$ reaction will be presented in the last section. In the following section, we briefly recall the main features of the time-independent QM (TIQM) method that we used to calculate the probabilities.

Quantum Mechanical Method

We have performed accurate three-dimensional QM calculations on the first excited $1^2A''$ PES for the $C(^3P) + OH(X^2\Pi) \rightarrow CO(a^3\Pi) + H(^2S)$ reaction at $J = 0$. We use a TIQM method that employs body−frame democratic hyperspherical coordinates.[16] This has already proved successful in describing atom−diatom insertion reactions, such as $N(^2D) + H_2 \rightarrow NH + H$,[17,18] $O(^1D) + H_2 \rightarrow OH + H$,[19,20] $C(^1D) + H_2 \rightarrow CH + H$,[21] $S(^1D) + H_2 \rightarrow SH + H$,[22] the O + OH reaction,[1−3] the H + O_2 reaction,[23,24] and also ultracold alkali−dialkali collisions.[25,26] At each hyperradius, ρ, we determined a set of eigenfunctions of a fixed-hyperradius reference Hamiltonian $H_0 = T + V$, which incorporates the kinetic energy, T, arising from deformation and rotation around the axis of least inertia at fixed hyperradius and the potential energy, V. At a small hyperradius, the adiabatic

† Part of the special section "30th Free Radical Symposium".

* Corresponding author. Email: pascal.honvault@univ-fcomte.fr.

10.1021/jp908963k
Published on Web 11/05/2009

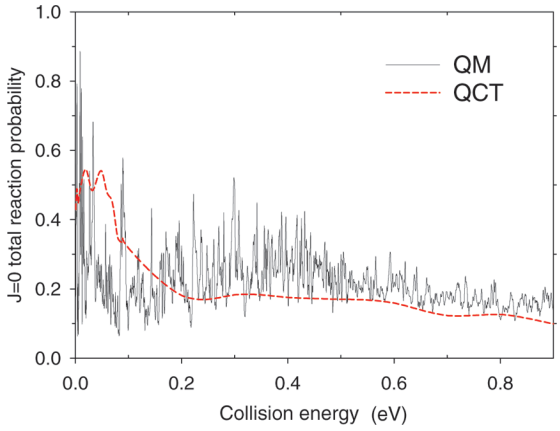

Figure 1. QM (—) and QCT (– – – –) total reaction probabilities as a function of the collision energy for the C + OH ($v = 0, j = 0$) → CO($a^3\Pi$) + H reaction.

states in each sector are expanded on the basis of pseudo-hyperspherical harmonics and span a large fraction of configuration space and allow for atom exchange. The coefficients of the expansion satisfy a set of second-order coupled differential equations with couplings arising from the difference between the exact Hamiltonian and the reference Hamiltonian. These coupled equations are solved using the Johnson−Manolopoulos log-derivative propagator.[27] The system C + OH is very difficult to study among the atom + OH reactions in quantum dynamics calculations because the three atoms are different, and so there is no permutation symmetry, in contrast with the O + OH system.[1−3] We essentially have to check two crucial parameters for convergence, the number of states (the size of the basis sets), and the asymptotic matching distance. For $J = 0$, the scattering wave function is expanded on the basis of 720 states dissociating at large hyperradius into the OH(23, 18, 13), CO(92, 87, 82, 76, 70, 63, 56, 47, 37, 23) and CH(14, 4) rovibrational sets (this notation indicates the largest rotational level, j, for each vibrational manifold, $v = 0-2$ for OH, $v = 0-9$ for CO, and $v = 0, 1$ for CH. The CH + O channel is always closed for the 0−0.9 eV collision energy range considered in the present work. The range of variation of the hyperradius is divided into 147 equal sectors between 2.9 and 21.1 a_0.

Results and Discussion

Total and state-to-state QM reaction probabilities have been computed for the C(^{3}P) + OH($X^2\Pi$) → CO($a^3\Pi$) + H(^{2}S) reaction at $J = 0$ in the 0−0.9 eV collision energy range on a regular grid with a step of 0.0005 eV. They are shown as a function of collision energy, E_c, in Figures 1, 2, and 3. The absence of barrier in the PES for the C + OH entrance arrangement leads to a total reaction probability $P^{J=0}$ that has no energy threshold, as was also the case for the probability obtained on the ground PES. The average reaction probability, which is high at very low energies, decreases as E_c increases, We observe a rising of the total $P^{J=0}$ as E_c rises between 0.2 and 0.4 eV, then a decrease between 0.4 and 0.53 eV and a constant around 0.19 above 0.53 eV. The increase above 0.2 eV is not due to the opening of product vibrational channels because the same behavior is found in the vibrationally state-resolved probabilities (Figure 2). The value of 0.19 at high E_c is relatively low, in contrast to the C + OH → CO($X^1\Sigma^+$) + H case,[13] for which $P^{J=0} \sim 1$. In the present case, the reactivity is not unity, indicating significant backscattering, as in the O + OH case.[4]

An extremely dense resonance structure is present at low collision energy, but the structure is less marked when E_c becomes higher. Some peaks are very intense and sharp. These quantum-mechanical resonances are associated with the deep HCO well in the potential energy surface, which leads to quasibound states. This is in strong contrast with the total reaction probability obtained on the ground PES for the C + OH reaction. A deep well is also involved, but the TDWP (or QCT) reaction probability[13] close to unity for all E_c is without any resonances. The small spurious oscillations at very low energies (see Figure 1 in ref 13) are due to the incomplete damping of the outgoing wave packet, particularly those with exceptionally long de Broglie wavelengths. Again, the very small exoergicity of the C(^{3}P) + OH($X^2\Pi$) → CO($a^3\Pi$) + H(^{2}S) reaction thus appears as an essential feature to obtain narrow resonances. Less product channels are available for the decay of these resonances which is therefore much slower than in the higher exoergic C(^{3}P)+ OH($X^2\Pi$) → CO($X^1\Sigma^+$) + H(^{2}S) reaction. The situation is similar to that found in the low exoergic (0.71 eV) O + OH reaction.[3] The shape is the same and peaks are very intense and sharp in the whole energy range considered here. The N + OH reaction probability[5] also presents the same shape but the resonances are much less pronounced because of the larger exoergicity (1.99 eV) of this reaction. So, the very small exoergicity of barrierless reactions involving a deep well appears as an essential feature to obtain narrow resonances.[21,22,28,30]

The QCT result reproduces the overall shape of the total QM reaction probability with a global decrease as E_c increases. However, the QCT method does not produce a good quantitative description of the QM reaction probability. As expected, the QCT reaction probability in Figure 1 does not show any sharp peak structure. In addition, the rising above 0.2 eV is not reproduced by the QCT method, giving a constant value of around 0.18 between 0.2 and 0.9 eV. Finally, the QCT reaction probability is significantly larger than the QM one at very low E_c and smaller above 0.2 eV. This is in contrast with the C + OH reaction on the ground PES, where a good agreement was found between the QCT and QM results.[13]

The vibrationally state-resolved reaction probabilities calculated at $J = 0$ in the 0−0.9 eV collision energy range are depicted in Figure 2. They are the rotation-summed reaction probabilities (summed over all open product rotational states). The shapes of the probabilities and the resonance structure are similar to those for the total reaction probability, with the exception of the vibrational state $v' = 3$ of CO($a^3\Pi$), for which a threshold appears around 0.08 eV where this channel becomes energetically accessible. For each v', the average reaction probability decreases as E_c increases. The sharp rising just above $E_c = 0$ eV already observed in the total reaction probability is present (of course, except for $v' = 3$). The resonance structure is dense below 0.53 eV, whereas it is less marked above this energy. The vibrationally state-resolved reaction probabilities present the same magnitude for all v' in the whole collision energy range (above the threshold for $v' = 3$), and none dominates the others.

Figure 3 shows some rotationally state-resolved reaction probabilities for CO($a^3\Pi$) ($v' = 0$) as a function of collision energy. They are characterized by a large number of very narrow peaks particularly at low energy. It is interesting to notice that Figure 3 shows a strong effect of the collision energy on the reactivity. At some collision energies, the reaction probability is even very small, reaching zero for a few E_c. The magnitudes of rotationally state-resolved reaction probabilities are similar.

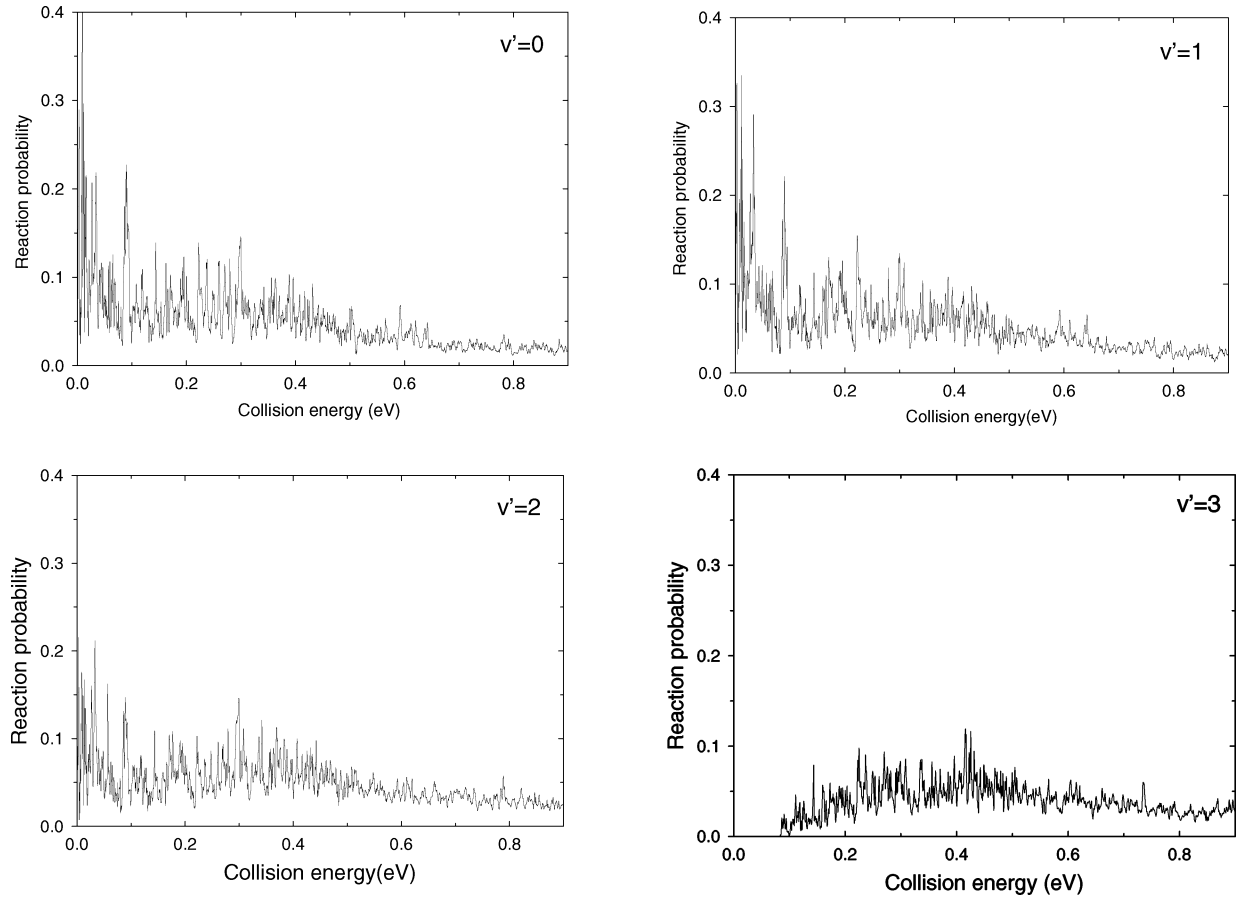

Figure 2. Vibrationally state-resolved probabilities as a function of the collision energy for the C + OH ($v = 0, j = 0$) → CO($a^3\Pi$) (v') + H reaction.

For all j', the resonance structure behaves as for the total and vibrationally state-resolved probabilities, even if the shapes are not the same: numerous pronounced resonances at low energy and broader small resonances at higher energy. There is an exception for $j' = 5$ where a pronounced resonance is observed at the relatively high energy 0.6715 eV. Finally, the rotationally state-resolved reaction probabilities do not depend strongly on the final rotational state j' of CO. Similar features are obtained for the other v'.

Vibrational distributions (reaction probability as a function of the CO($a^3\Pi$) quantum vibrational number v') at $J = 0$ are plotted in Figure 4 at four collision energies: 0.01, 0.05, 0.1, and 0.5 eV. The distributions do not show well-defined behaviors. For the two lowest energies, the distributions appear slightly inverted, the reaction probability for $v' = 0$ being slightly smaller than that for $v' = 1$. At the other energies, a flat behavior is found with the same reaction probability for all v', except for the highest ($v' = 3$ at 0.1 eV and $v' = 4$ at 0.5 eV). These features between a marked inverted distribution and a purely statistical distribution are consistent with a reaction that involves both direct (COH complex) and indirect (HCO complex) mechanisms, as in the N + OH case.[5] This is again in contrast with the QM (and QCT) results obtained on the ground PES for C + OH which gives a very strong vibrational population inversion related to a direct mechanism.[10,13] The situation is also different from that found for O + OH, where a statistical distribution was found,[4] that is, the probability decreases when v' increases, the most populated vibrational level being $v' = 0$.

In Figure 5, we plot the rotational distributions (reaction probability as a function of the CO($a^3\Pi$) rotational quantum number j') for CO ($v' = 0$) at four collision energies: 0.01, 0.05, 0.1, and 0.5 eV. The distributions show an oscillatory structure at all E_c. From 0.01 to 0.5 eV, the distributions are neither rotationally hot nor rotationally cold because low, medium, and high j' are similarly populated. Again, the present QM distributions totally differ from the QM ones computed at $J = 0$ for the CO($X^1\Sigma^+$) products,[13] where the oscillations are less pronounced and the low and medium j' are the most populated. They are similar to those for N + OH[5] for collision energies below 0.1 eV, but are completely different at higher E_c, for which the high j' are preferred for the NO products. An interesting feature exhibited in Figure 5 is that the rotational selectivity is very strong. Not all accessible rotational states are populated (for instance, the probability is nearly zero at 0.1 eV for $j' = 5$, 23, and 35), whereas only a few rotational states are highly populated. When E_c goes from 0.01 to 0.5 eV, the shape of the distributions does not change.

The rate constant for OH($v = 0, j = 0$) is obtained using the exact TIQM reaction probability for $J = 0$, and the reaction probabilities for $J > 0$ are calculated in the J-shifting approach.[29] We have already used this procedure in the barrierless O + OH[1,31] and N + NO[30] reactions. The rate constant, including the temperature-dependent electronic factor[32] as a function of temperature, is displayed in Figure 6. It varies from 4.47 10^{-12} cm^3 s^{-1} at 10 K to 2.14 10^{-11} cm^3 s^{-1} at 500 K with a maximum value of 4.47 10^{-11} cm^3 s^{-1} obtained at 90 K, so the reaction is fast in a wide temperature range. The TIQM result is also compared with the QCT prediction.[11] The TIQM and QCT rate constants are in good agreement. In particular, the temperature dependence is the same between the two methods. However, quantitatively, some disagreement appears. The increase at low

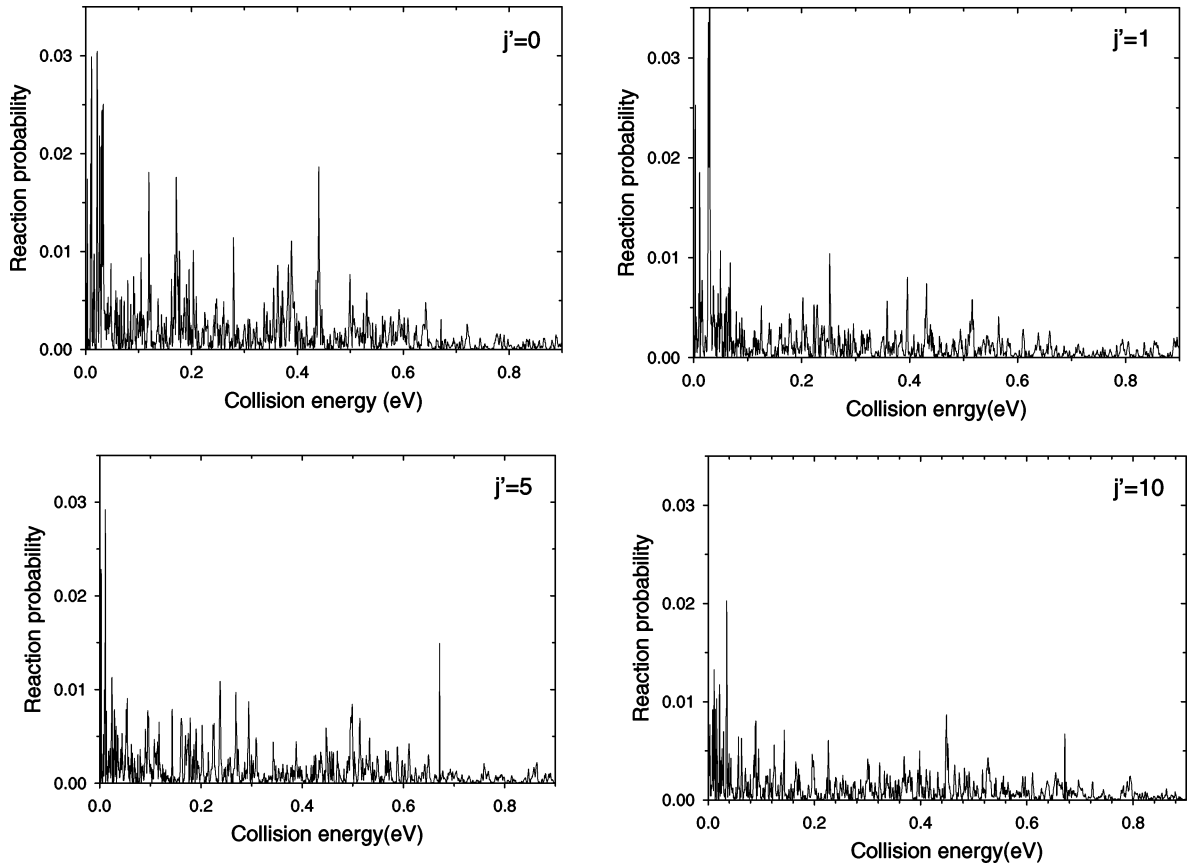

Figure 3. Rotationally state-resolved probabilities as a function of the collision energy for the C + OH ($v = 0, j = 0$) → CO($a^3\Pi$) ($v' = 0, j'$) + H reaction.

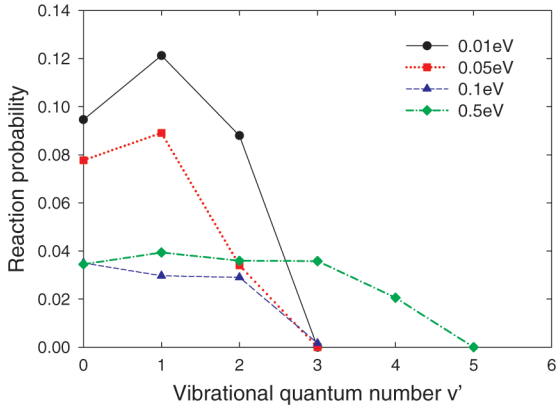

Figure 4. Product vibrational distributions: vibrationally state-resolved reaction probabilities as a function of vibrational quantum number v' of CO($a^3\Pi$) at 0.01 (—, black), 0.05 (••••, red), 0.1 (— — — —, blue), and 0.5 eV (•—•—, green).

temperature is sharper for the QCT result, yielding a slight overestimate of the TIQM value in the 10−100 K temperature range. After the maximum, the QCT decrease is slower, yielding again an overestimate of the TIQM result above 130 K. This disagreement may be linked to the QCT method, which is based on classical mechanics, so the zero-point energy is not rigorously accounted and quantum effects cannot occur. Of course, the TIQM rate constant has been calculated using the J-shifting approximation, which might not be accurate in the present case, where a dense resonance structure was found in the $J = 0$ reaction probability. As already mentioned in detail in ref 11, the temperature dependence found on the $1^2A''$ excited electronic state is totally different from that found for the X^2A' ground electronic state, where the rate constant always decreases from 10 K, showing no maximum between 10 and 500 K.

Conclusions

We have carried out dynamical calculations of the C(^{3}P) + OH($X^2\Pi$) → CO($a^3\Pi$) + H(^{2}S) reaction by means of an accurate TIQM method. Exact total and state-to-state QM reaction probabilities have been computed at $J = 0$ using the ab initio PES built by our group.[11]

The TIQM total reaction probability calculated for collision energies from 0 to 0.9 eV shows a dense resonance structure due to long-lived resonances supported by the HCO potential well. It decreases globally with the collision energy and is in good agreement with the QCT prediction. The result is different from that obtained on the ground PES using a TDWP method,[13] where the probability was unity. The vibrationally state-resolved reaction probabilities reproduce the features seen in the total reaction probability. Reaction probabilities for specific product rotational states have also been computed. The resonances are narrower, as expected, and a strong effect of the collision energy on the reactivity has been found.

The product vibrational quantum state distributions are slightly inverted at 0.01 and 0.05 eV, whereas they are rather flat at 0.1 and 0.5 eV, showing that both direct and indirect mechanisms are involved. Product rotational distributions determined at four collision energies—0.01, 0.05, 0.1, and 0.5 eV—show a specific behavior with respect to j' (some j' are not populated), but low, medium, and high j' can be populated. The shapes of the vibrational and rotational distributions are totally different from those found on the ground PES.

QM calculations for $J > 0$ are computationally extremely expensive, so the present study was limited to $J = 0$. However,

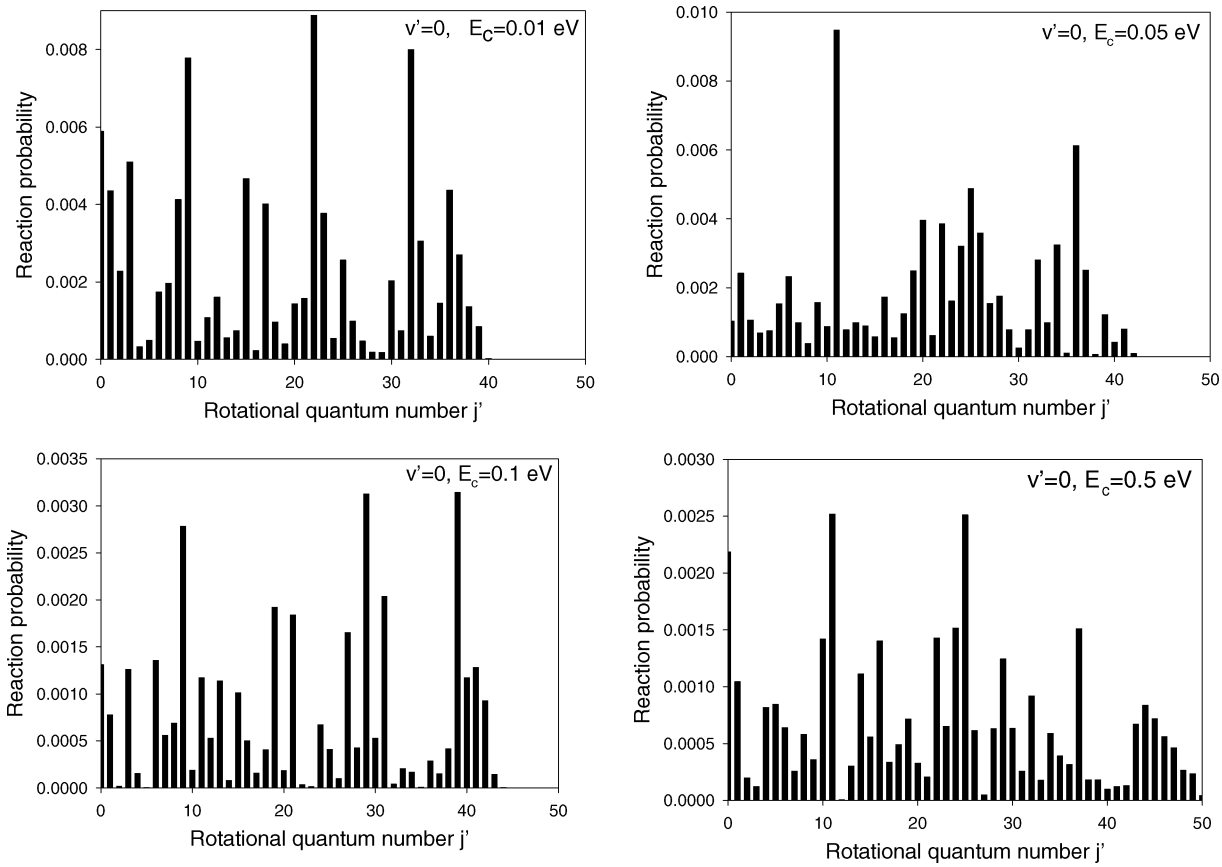

Figure 5. Product rotational distributions: rotationally state-resolved reaction probabilities as a function of rotational quantum number, j', of CO($a^3\Pi$) ($v' = 0$) at 0.01, 0.05, 0.1, and 0.5 eV.

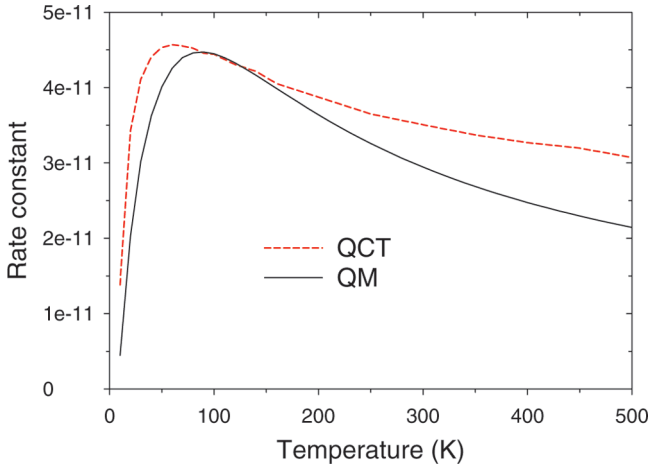

Figure 6. QM (solid line) and QCT (dashed line) rate constants (in $cm^3\ s^{-1}$ $molecule^{-1}$) for the C + OH ($v = 0, j = 0$) → CO($a^3\Pi$) + H reaction.

using the exact $J = 0$ reaction probability and a J-shifting method for $J > 0$, the rate constant for OH ($v = 0, j = 0$) has also been computed in the 10−500 K temperature range. The QM rate constant is large, even at low temperatures, and is in good agreement with the QCT rate constant recently calculated in our group.[11]

Finally, the results reported here suggest that the dynamics on the $1^2A''$ first excited state of COH is totally different from that on the X^2A' ground PES. A full understanding of the dynamics of the C + OH reaction has therefore to take into account the excited electronic states.

In the future, we plan to remove the J-shifting approximation by calculating the TIQM reaction probabilities for $J > 0$ to obtain other product state-resolved information, such as the state-to-state differential sections. We would also like to study the effect of the initial rotational and vibrational excitations in the OH reactant on the reactivity.

Acknowledgment. We acknowledge support from the Programme National Physique Chimie du Milieu Interstellaire (INSU/CNRS) and from the Pole de Sciences Planetaires of Bourgogne Franche-Comte. This work was performed using HPC resources from GENCI [CCRT/CINES/IDRIS] (Grant 2009 [i2009082031]).

References and Notes

(1) Xu, C.; Xie, D.; Honvault, P.; Lin, S. Y.; Guo, H. *J. Chem. Phys.* **2007**, *127*, 024304.
(2) Lin, S. Y.; Guo, H.; Honvault, P.; Xu, C.; Xie, D. *J. Chem. Phys.* **2008**, *128*, 014303.
(3) Jorfi, M.; Honvault, P.; Halvick, P.; Lin, S. Y.; Guo, H. *Chem. Phys. Lett.* **2008**, *462*, 53.
(4) Jorfi, M.; Honvault, P.; Bargueno, P.; González-Lezana, T.; Larrégaray, P.; Bonnet, L.; Halvick, P. *J. Chem. Phys.* **2009**, *130*, 184301.
(5) Jorfi, M.; Honvault, P. *J. Phys. Chem. A* **2009**, *113*, 2316.
(6) Jorfi, M.; Honvault, P.; Halvick, P. *Chem. Phys. Lett.* **2009**, *471*, 65.
(7) Jorfi, M.; Honvault, P.; Halvick, P. *J. Chem. Phys.* **2009**, *131*, 094302.
(8) Zanchet, A.; Bussery-Honvault, B.; Honvault, P. *J. Phys. Chem. A* **2006**, *110*, 12017.
(9) Zanchet, A.; Halvick, P.; Rayez, J.-C.; Bussery-Honvault, B.; Honvault, P. *J. Chem. Phys.* **2007**, *126*, 184308.
(10) Zanchet, A.; Halvick, P.; Bussery-Honvault, B.; Honvault, P. *J. Chem. Phys.* **2008**, *128*, 204301.
(11) Zanchet, A.; Bussery-Honvault, B.; Jorfi, M.; Honvault, P. *Phys. Chem. Chem. Phys.* **2009**, *11*, 6182.
(12) Lin, S. Y.; Guo, H.; Honvault, P. *Chem. Phys. Lett.* **2008**, *453*, 140.

(13) Bulut, N.; Zanchet, A.; Honvault, P.; Bussery-Honvault, B.; Banares, L. *J. Chem. Phys.* **2009**, *130*, 194303.
(14) Neyer, D. W.; Luo, X.; Burak, I.; Houston, P. L. *J. Chem. Phys.* **1995**, *102*, 1645.
(15) Loettgers, A.; Untch, A.; Keller, H.-M.; Schinke, R.; Werner, H.-J.; Bauer, C.; Rosmus, P. *J. Chem. Phys.* **1997**, *106*, 3186.
(16) Honvault, P.; Launay, J.-M. *Theory of Chemical Reaction Dynamics*; Lagana, A., Lendvay, G., Eds.; Kluwer: Dordrecht, The Netherlands, 2004; p 187.
(17) Honvault, P.; Launay, J. M. *J. Chem. Phys.* **1999**, *111*, 6665.
(18) Balucani, N.; Cartechini, L.; Capozza, G.; Segoloni, E.; Casavecchia, P.; Volpi, G. G.; Aoiz, F. J.; Banares, L.; Honvault, P.; Launay, J.-M. *Phys. Rev. Lett.* **2002**, *89*, 013201.
(19) Honvault, P.; Launay, J.-M. *J. Chem. Phys.* **2001**, *114*, 1057.
(20) Aoiz, F. J.; Banares, L.; Castillo, J. F.; Vallance, C.; Denzer, W.; Brouard, M.; Honvault, P.; Launay, J.-M.; Dobbyn, A. J.; Knowles, P. J. *Phys. Rev. Lett.* **2001**, *86*, 1729.
(21) Banares, L.; Aoiz, F. J.; Honvault, P.; Bussery-Honvault, B.; Launay, J.-M. *J. Chem. Phys.* **2003**, *118*, 565.
(22) Banares, L.; Castillo, J. F.; Honvault, P.; Launay, J.-M. *Phys. Chem. Chem. Phys.* **2005**, *7*, 627.
(23) Lin, S. Y.; Guo, H.; Honvault, P.; Xie, D. *J. Phys. Chem. B* **2006**, *110*, 23641.
(24) Honvault, P.; Lin, S. Y.; Xie, D.; Guo, H. *J. Phys. Chem. A* **2007**, *111*, 5349.
(25) Soldàn, P.; Cvitas, M. T.; Hutson, J. M.; Honvault, P.; Launay, J.-M. *Phys. Rev. Lett.* **2002**, *89*, 153201.
(26) Cvitas, M. T.; Soldàn, P.; Hutson, J. M.; Honvault, P.; Launay, J. M. *Phys. Rev. Lett.* **2005**, *94*, 033201.
(27) Manolopoulos, D. E. *J. Chem. Phys.* **1986**, *85*, 6425.
(28) Rackham, E. J.; González-Lezana, T.; Manolopoulos, D. E. *J. Chem. Phys.* **2003**, *119*, 12895.
(29) Bowman, J. M. *J. Phys. Chem.* **1991**, *95*, 4960.
(30) Jorfi, M.; Honvault, P. *J. Phys. Chem. A*, in press.
(31) Lique, F.; Jorfi, M.; Honvault, P.; Halvick, P.; Lin, S. Y.; Guo, H.; Xie, D.; Klos, J.; Dagdigian, P. J.; Alexander, M. H. Submitted.
(32) Graff, M. M.; Wagner, A. F. *J. Chem. Phys.* **1990**, *92*, 2423.

JP908963K